Egyptian Geophysical Society
EGS Journal, Vol. 15, No. 1, 139-153 (2017)

STRUCTURAL INTERPRETATION OF AIRBORNE RADIOMETRIC AND MAGNETIC SURVEY DATA, WADI TIMSAH AREA, SOUTHERN EASTERN DESERT, EGYPT

M.E. Abdelrazik and A.M. Abu-Donia

Nuclear Materials Authority, P.O. Box 530, El-Maadi, Cairo, Egypt

التفسير البنائي للمعطيات الجوية الإشعاعية والمغناطيسية لمنطقة وادي التمساح، الصحراء الشرقية الجنوبية، مصر

الخلاصـــة: تم استخدام معطيات المسح الجوي الإشعاعي والمغناطيسي لمنطقة وادى التمساح بالصحراء الشرقية الجنوبية لمصر وذلك للاستدلال على التراكيب الجيولوجية السطحية وتحت السطحية، وتحديد النطاقات الشاذة إشعاعيا.

أوضحت نتائج المعطيات الإشعاعية ارتباط القراءات الإشعاعية العالية بصخور الجرانيت الحديث حيث تمثل النطاقات الشاذة، والتي غالبا ما تتوافق مع الفوالق والشقوق المؤثرة لمنطقة الدراسة. من خلال تطبيق تقنية طيف الطاقة للبيانات المغناطيسية, أمكن تحديد متوسط الأعماق للأجسام المسببة للشاذات المغناطيسية الضحلة والعميقة وهى ١،١٠ و ٢,٦٥ كم على الترتيب.

ساعد هذا الترشيح كذلك في الفصل بين الشاذات المغناطيسية الضحلة والعميقة, وتم رسم الخرائط لهاتين المركبتين. تحقق التفسير التركيبي للبيانـــات المغناطيسية الجوية من خلال تطبيق تقنيات التفسير المتقدمة التي تمكننا من التحديد التلقائي، وتقدير أعماق التراكيب المغناطيسية وتشمل هذه التقنيات المشتقة الأفقية ومعادلة تجانس أويلر.

أكدت نتائج كل من الطريقتين تكاملهما معا، في ظل الافتراض من راسية (عمودية) خطوط التماس لمصادر الشاذات. تقدر الأعماق المستنتجة بطريقة أويلر حوالى ٢١٥ متر وذلك للتراكيب الجيولوجية الضحلة، أما التراكيب الجيولوجية العميقة فتصل الى حوالى ٢٨٠٠ مترا.

ويكشف تكامل نتائج معطيات المسح الجوي الإشعاعي والمغناطيسي أن معظم الشاذات الإشعاعية في منطقة الدراسة مرتبطة بصخور الجرانيت الحديث وممتدة في اتجاهات شمال الشرق - جنوب الغرب، شمال شمال الشرق – جنوب جنوب الغرب، شمال الغرب – جنوب الشرق، وغرب شمال الغرب – شرق جنوب الشرق.

ABSTRACT: The airborne radiometric and magnetic survey data in Wadi Timsah area, Southern Eastern Desert, Egypt, were used to deduce the surface and the subsurface structural lineaments. Besides, they are utilized to identify the anomalous radioactive zones. The results of radiometric data delineated anomalous zones, mostly connected with younger granites that seem to be structurally controlled. The dominated fault system appears to play the most effective role in the structural framework of the study area. Two main average magnetic interfaces at depths 1.10 and 2.65 km were deduced through the application of the two-dimensional power spectrum technique. Filtering assisted in the discrimination between residual (shallow-seated) and regional (deep-seated) magnetic components. Structural interpretation of the aeromagnetic data was achieved through the application of advanced techniques, that provide estimation of the depths of magnetic structures. These techniques include Horizontal Gradient Magnitude (HGM) and Euler deconvolution. The results of the two methods confirm each other, under the assumption of vertical contacts of anomalous sources and features of linear segments. The estimated depths varied between 215 m for the near-surface structures and 2800 m for the deep-seated ones. The integration of results of the aeroradiometric and aeromagnetic interpretations revealed that most of the recorded radiometric anomalies lie over younger granites, which are distributed as isolated bodies aligned around huge mother batholith. This batholith is dissected mainly by NE-SW, NNE-SSW, NW-SE and WNW-ESE structural lineaments.

INTRODUCTION

The study area is located to the east of the River Nile Valley, southeast of Aswan city and at the central part of the southern Eastern Desert of Egypt (Fig. 1). It is bounded by latitudes 23° 02` 43`` and 23° 26` 50`` N, and longitudes 33° 48` 04`` and 34° 27` 13``E. The study area is mainly covered by Precambrian igneous and metamorphic rocks, that overlain by Upper Cretaceous undifferentiated Phanerozoic sediments. These rock exposures are traversed by several Wadis (dry valleys) filled with Quaternary sediments. The present study aims to throw light on the surface and subsurface lithologic and structural features that affecting the framework of the study area, and detect any relation that might exist between the sites of radioactive anomalies and the prevailing structural trends.

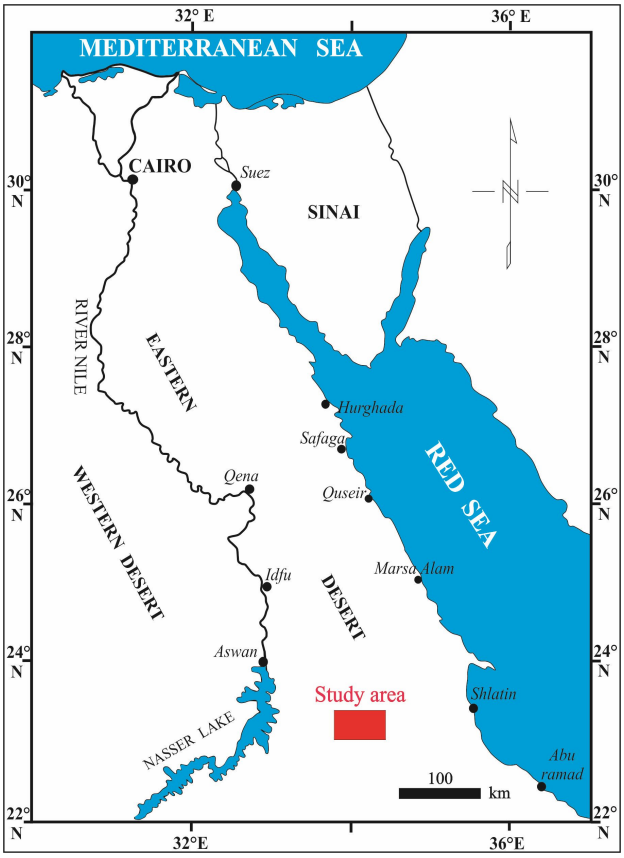

Fig. (1): Location map of Wadi Timsah area, Southern Eastern Desert, Egypt.

GEOLOGIC SETTING

The study area represents a part of Late Proterozoic–Early Palaeozoic Pan-African Orogeny, forming the Arabian-Nubian shield (950–450 Ma; Kroner, 1984). The exposed rocks (Fig. 2) are chronologically grouped into the following tectonic-stratigraphic units, according to the classification of El-Gaby et al. (1990), starting from the oldest):

1- Ophiolite Sequence:

The ophiolite rocks are represented by serpentinites, talc carbonates, schists, amphibolites and gabbros, located at the north central part of the study area.

2- Arc Assemblage:

A- Metasediments:

These constitute the most extensively outcropping unit in the basement rocks of Egypt, except for the granites (Hassan and Hashad, 1990). These rocks are mainly composed of muscovite-biotite metapsommite, semipelite and pelite, with minor units of intermediate to acidic volcanics and cherts, locally schistose, mylonitic and granitic hybridised. These metasediments are exposed to the north and south of the west central part of the study area (EGSMA, 1996).

B- Metavolcanics:

These cover a vast area in the central, western and southern parts of the study area. These rocks are generally thick bodies and range in composition from ultrabasic and intermediate (andesite) to acidic (dacites or even rhyolites), and may be island-arc volcanics (El-Shazly, 1977).

3- Intrusive Rocks:

These include the granitic intrusions of the older granites (granodiorites) and younger granites (monzo-granites and alkali-feldspar granites). The older granites cover a wide area and occur mainly at the central parts of the study area. These rocks range in composition from hornblende tonalites and granodiorites, locally with potash feldspar mega-crysts (Fig. 2), (Phillips, 2000).

Younger granites are encountered in the southeastern part of Gabal Shiqaqat and the southern part at Gabal (G.) Rahayah. These rocks are composed of muscovite monzo-granites and alkali-feldspar granites.

4- The Phanerozoic Sediments:

The Phanerozoic sediments of the study area are represented by Mesozoic sediments. These are formed of bedded sandstone, conglomerate, siltstone and mudstone (Fig. 2). These are located at the northeastern and northwestern parts of the study area, and unconformably overlie basement rocks.

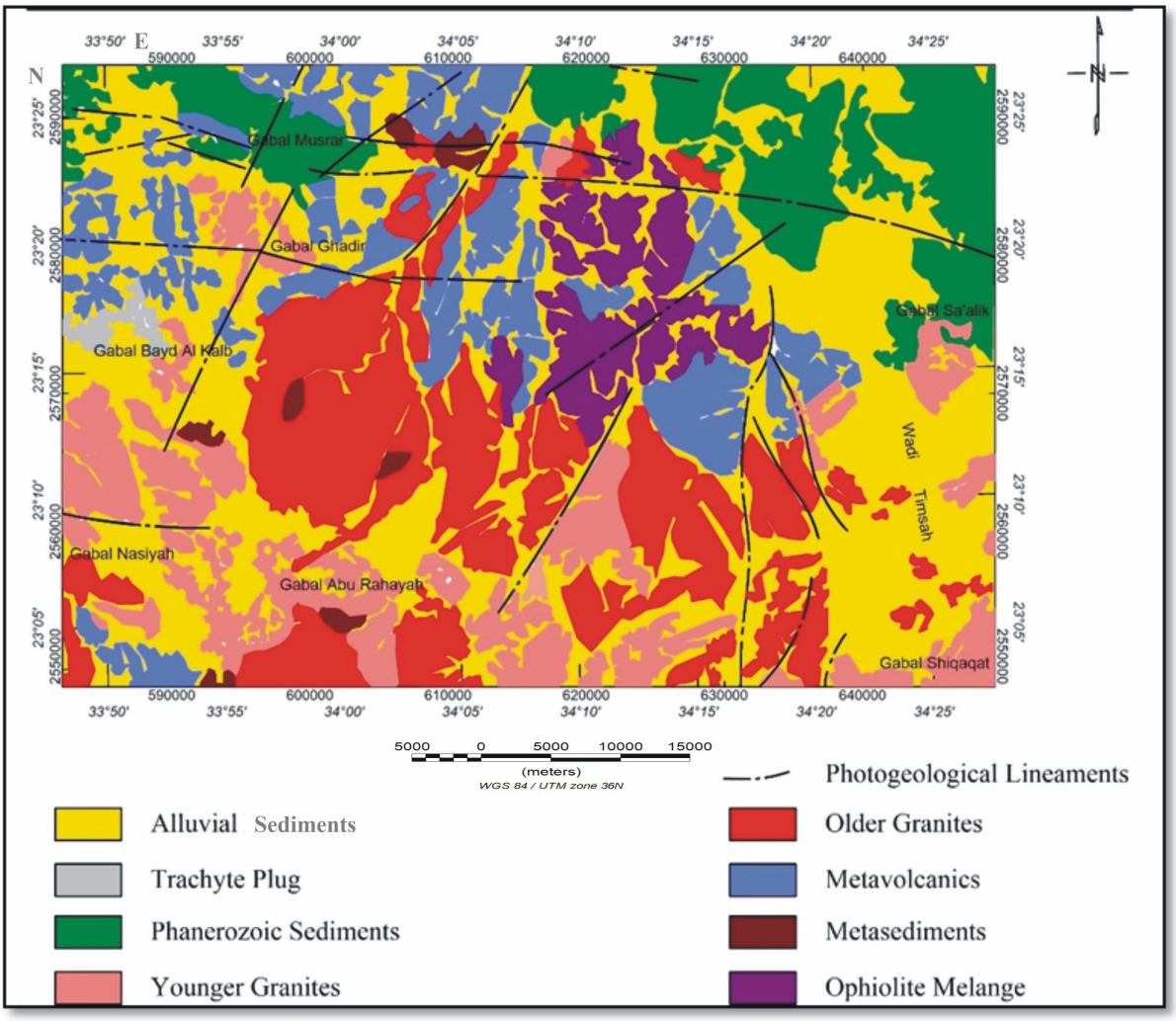

Fig. 2: Geologic map of Wadi Timsah area, Southern Eastern Desert, Egypt (EGSMA, 1996).

5- Trachyte Plugs:

Quartz trachyte plugs are encountered in the western part of the study area at Gabal Bayd Al Kalb.

6- Alluvial Sediments:

The Quaternary alluvial sediments are composed of Wadi alluvium, sand, as well as gravel fill and terraces.

AIRBORNE GEOPHYSICAL DATA

The study area was involved in the extensive airborne magnetic and gamma-ray spectrometric surveys, conducted by Aero- Service Division, Western Geophysical Company of America, USA, in 1984. These surveys covered a large segment of the Southern Central and Northern Red Sea Hills of the Eastern Desert of Egypt, as a part of the Mineral, Petroleum and Groundwater Assessment Program (MPGAP) (Aero-Service, 1984). Both surveys were conducted along nearly parallel flight lines oriented in the NE-SW direction, almost perpendicular to the major predominant structures and 1.5 km spacing intervals. Meanwhile, the tie lines were flown in the NW-SE direction at 10 km intervals.

Analysis and integration of these data, conducted over the study area, enabled to infer accurately the most pronounced structural trends both on the surface, shallow and at deeper depths. Moreover, such data were utilized to detect any relation, that might exist between the locations of radiometric anomalies and the interpreted structural trends.

1. Aeroradiometric Survey Data:

The total-count aero-radiometric measurements, registered over the study area (Fig. 3), range from about 1.12 Ur over the metavolcanics to 20.8 Ur over the younger granites. Simple techniques of statistical analysis were applied to the aeroradiometric survey data to determine the backgrounds of the separated lithologic and/ or interpreted radiometric units, and locate the radioactive anomalous zones. The arithmetic mean (X) and the standard deviation (S) of aerial radioactivity were computed for these units. The results of statistical analysis are shown on table (1).

Table (1): Results of statistical treatment for the T.C. aeroradiometric data of various rock units (in Ur*10) of Wadi Timsah area, Southern Eastern Desert, Egypt.

Rock type	No.	Min.	Max.	X	S
Alluvial sediments	894	14.4	144	72	27
Quartz trachyte plugs	7	32	96	80.7	9.9
Phanerozoic Sediments	212	12.8	112	42.5	16.3
Younger Granites	233	22.4	208	109	42.5
Older Granites	354	35.2	176	98	28
Ophiolite Melange	91	22.4	80	42	13.2
Metavolcanics	201	11.2	166.4	65.7	30.3
Metasediments	12	28.8	144	102.7	35.6

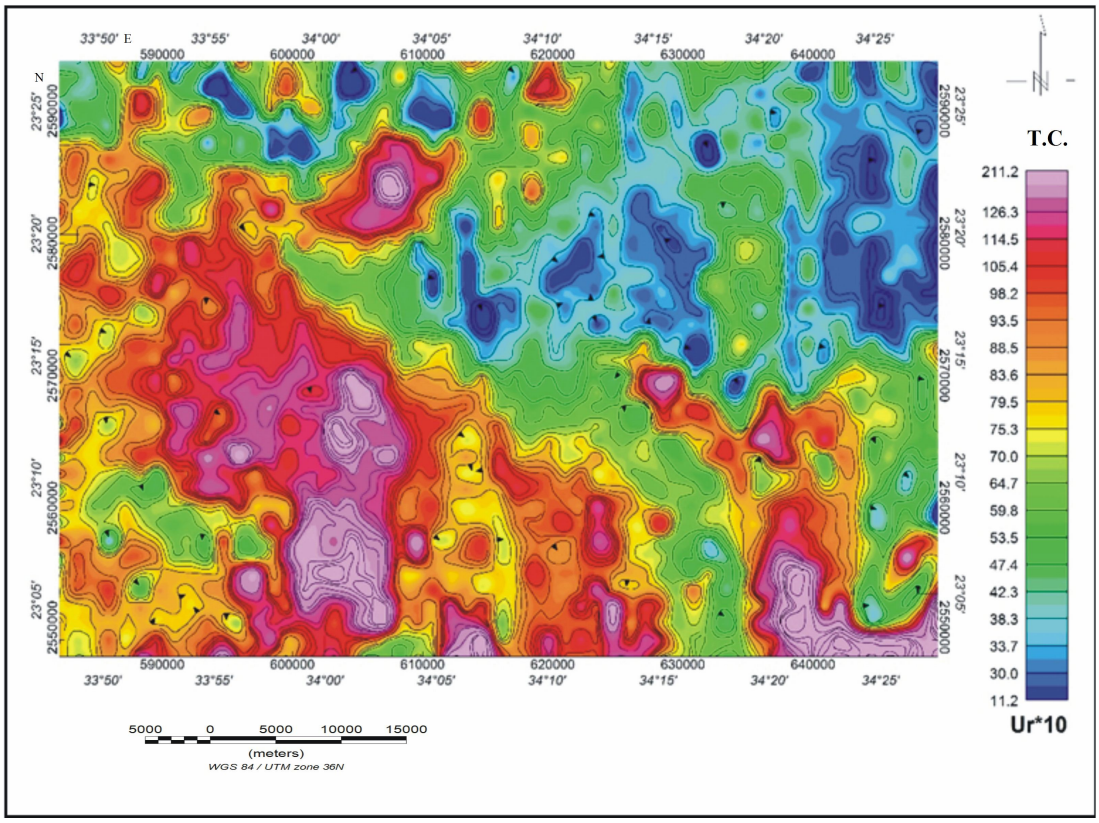

Fig. 3: Total-count (T.C.) aero-radiometric contour map (in Ur*10) of Wadi Timsah area, Southern Eastern Desert, Egypt (Aero-Service, 1984).

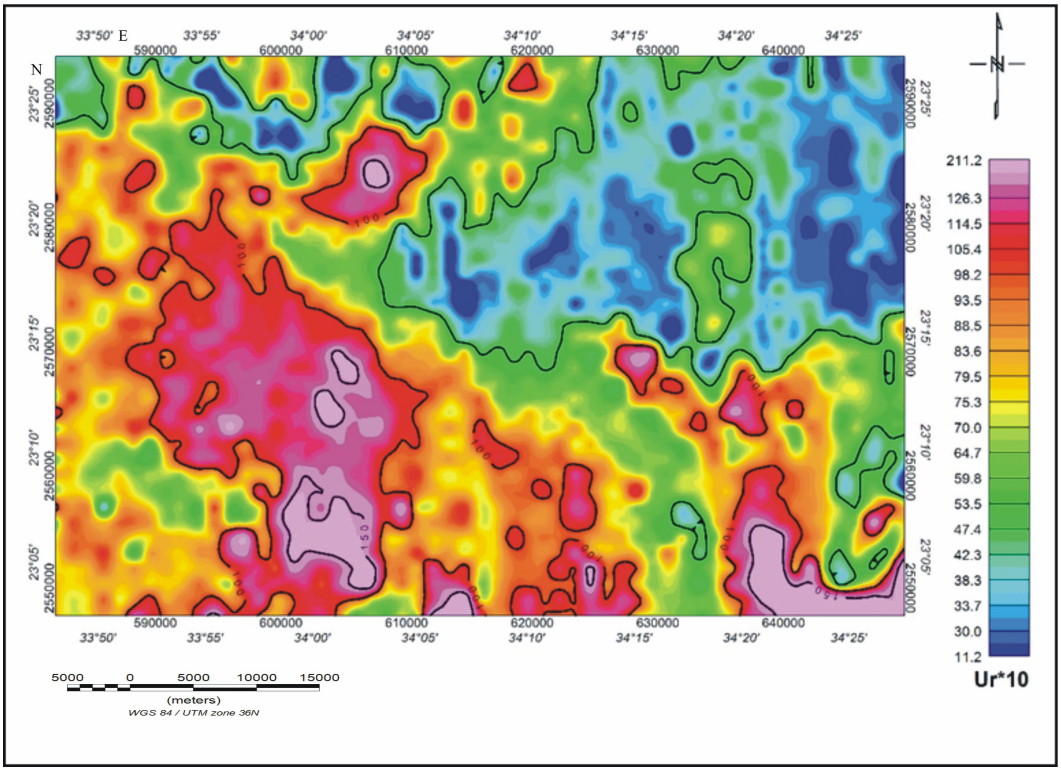

Fig. 4: Total-count (T.C.) aero-radiometric zonation map (in Ur*10) of Wadi Timsah area, Southern Eastern Desert, Egypt.

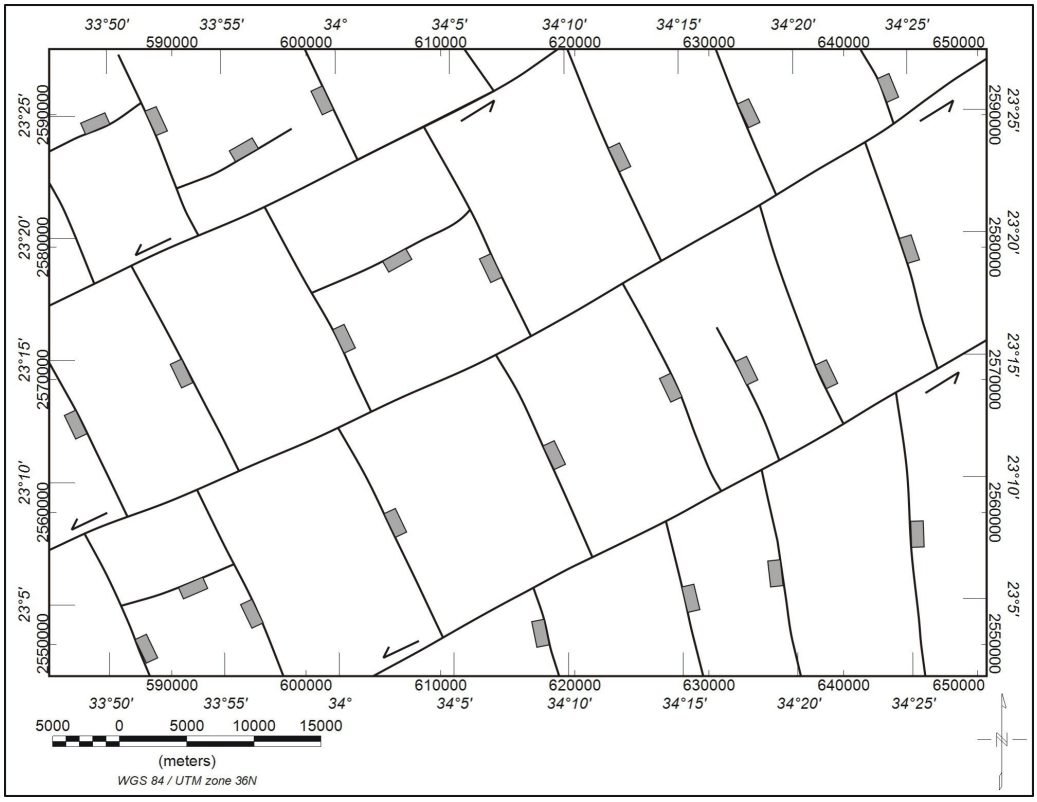

Fig. 5: Near-surface structures, as inferred from the total count aeroradiometric map, Wadi Timsah area, Southern Eastern Desert, Egypt.

From the study of the aero-radiometric survey data, three main levels of radioactivities were generally distinguished. These levels were used to construct the aerial radiometric zonation map (Fig. 4). They are summarized in the following:

A- Low radioactivity level (less than 5 Ur):

This level extends over a wide area at the northern and eastern parts of the study area. It is associated mainly with ophiolite mélange, metavolcanics, metasediments and Phanerozoic sediments.

B- Intermediate radioactivity level (from 5 Ur to 15 Ur):

It is recorded over the western and south central parts of the study area. It is mainly related to older granites (tonalites) and alkali-feldspar granites.

Min.= minimum; Max.= maximum; X= arithmetic mean; S= standard deviation and No. is the number of measurements.

Many major lineaments could be traced from the elongations of the radiometric anomalies (Fig. 3). As illustration in (Fig. 5), these trends follow the NE-SW and NW-SE directions. Accordingly, they seem to be the most important trends, which play the most effective role in the structural framework and radioactive mineral emplacement in the study area. Some other minor trends N-S and NNW-SSE, could also be followed from some other elongated bodies of the radioactive anomalies.

2. Aeromagnetic Survey Data:

2.1. Magnetic data processing:

Processing of potential field data entails the application of various filters to the data, in order to accentuate the features that will aid in the interpretation of such data. The total field intensity of aeromagnetic anomaly map (Fig. 6) was processed and prepared for analysis and interpretation. It was reduced to the northern magnetic pole of the earth (RTP) (Fig. 7), using the magnetic inclination of 31.7° and a declination of 1.95°. The RTP method reduced the effect of the earth's ambient magnetic field and provided a more accurate determination of the positions of anomalous sources.

The RTP aeromagnetic anomaly map (Fig. 7) shows low and high-frequency magnetic anomalies, distributed allover the study area. The elongated positive magnetic anomalies having maximum values and exposed at notable locations, occupying the western, southeastern and northeastern parts of the study area. These anomalies are characterized by high-frequency and high-amplitude, and trending in the N-S, NNW-SSE and ENE-SWS directions. The local variations of the frequencies and amplitudes of the magnetic anomalies within each zone may be due to either the differences in their petrographic compositions or the differences in relative depths of their sources. Close to the central part of the study area and towards its northwestern part, some magnetic anomalies of low frequencies and low amplitudes are seen. They may reflect their considerable depths in their causative sources, trending in the NNW-SSE direction.

Magnetic data observed in the geophysical surveys are the sum of magnetic effects produced by all the underground sources. The targets for such specific surveys are often small-scale structures, that occur at shallow depths. The magnetic responses of these targets are embedded in a regional field, which arises from magnetic sources usually larger or deeper than these targets. Correct estimation and removal of the regional field from the initial effect yields the residual responses produced by the target sources.

In the present study, the Fast Fourier Transform (FFT) was applied on the RTP magnetic data (Fig. 8), using Oasis montaj package (Geosoft program, 2007), to explore their frequency content and select the suitable cut-off frequency for carrying out both the high-pass and low-pass filtered maps. As a result of the visual inspection of the two-dimensional power spectrum curves (Fig. 8), two linear segments were distinguished and fitted. The first segment lies at the low frequency (long wavelength) side with a steep slope and is related to the deep and/or broad causative magnetic sources. Meanwhile, the second segment is located at the high frequency (short wavelength) side with a gentle slope, due to relatively shallow sources. The slope of a line fitted to each of the first and second segments of the spectrum curve is used to estimate the average depths of the regional and residual sources. The depths of an ensemble of sources are easily determined by measuring the slope of the energy (power) spectrum and dividing by 4π. A typical energy spectrum for the magnetic data may exhibit three parts, which are deep source component, shallow source component and noise (white) component.

The inspection of the power spectrum curve of the study area reveals that, the deep-seated magnetic component is distinguished by a frequency band, that ranges from 0.0 to 0.2 cycle/grid unit. Meanwhile, the frequencies of the near-surface magnetic component vary between 0.2 and 0.6 cycle/grid unit (Fig. 8).

These bands of frequencies were used to produce the high-pass (residual) and low-pass (regional) maps (Figs. 9a and 10a), respectively, using the band-pass filter technique (Geosoft program, 2007). The estimated average depths for the shallow and deep magnetic sources, as calculated from the power spectrum curve, are 1.10 km and 2.65 km, respectively.

The residual magnetic anomalies can be defined as the anomalies, that are economically interesting, because they indicate shallow bodies and are characterized by weaker and more localized anomalies, which are superimposed on the regional magnetic pattern, as high-frequency anomalies.

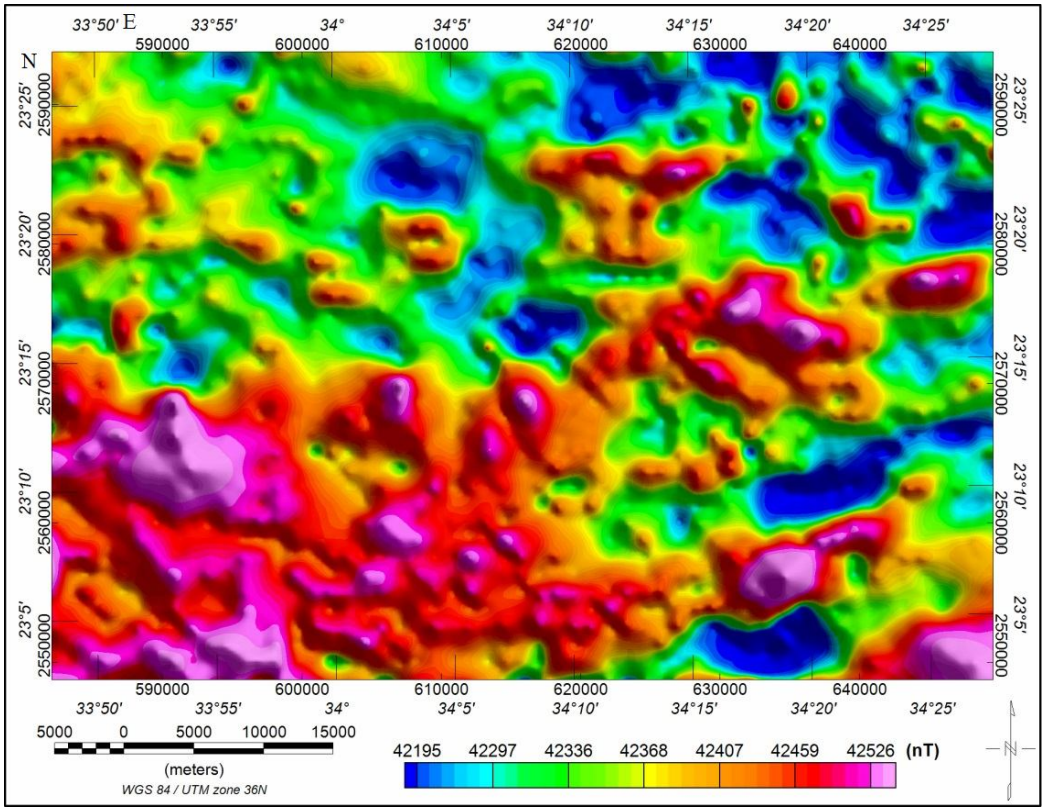

Fig. 6: Aeromagnetic field-intensity map of Wadi Timsah area, Southern Eastern Desert, Egypt (Aero-Service, 1984).

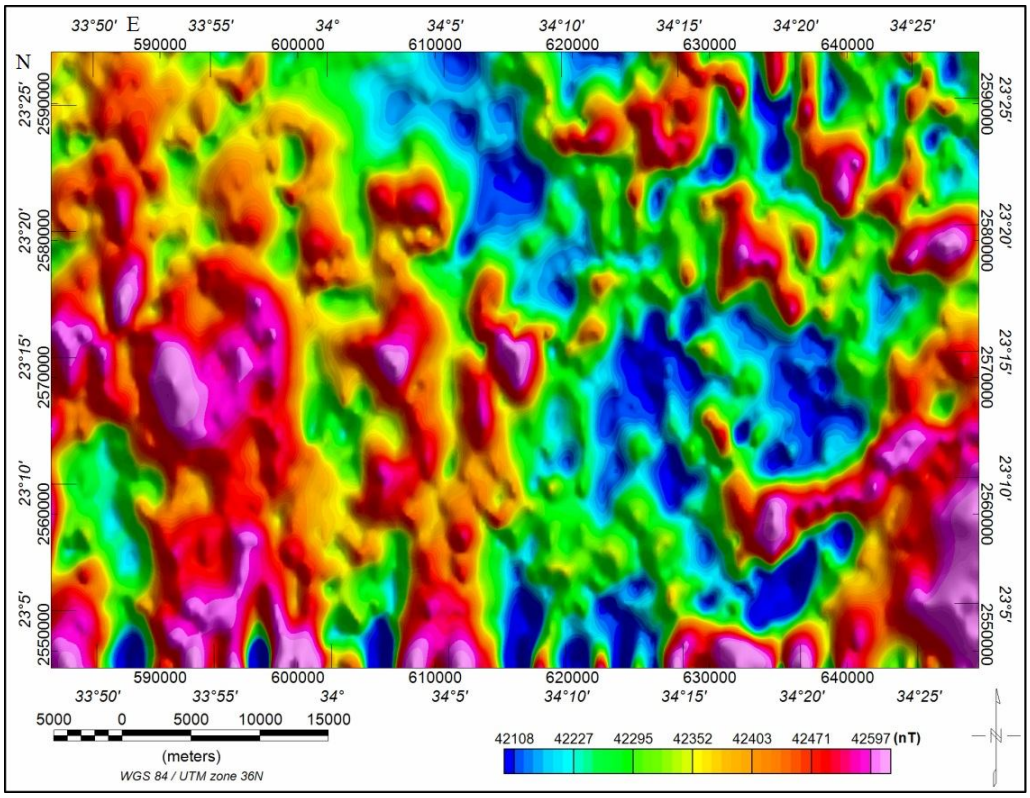

Fig. 7: Reduced to the Northern-Pole (RTP) aeromagnetic field-intensity map (RTP), Wadi Timsah area, Southern Eastern Desert, Egypt.

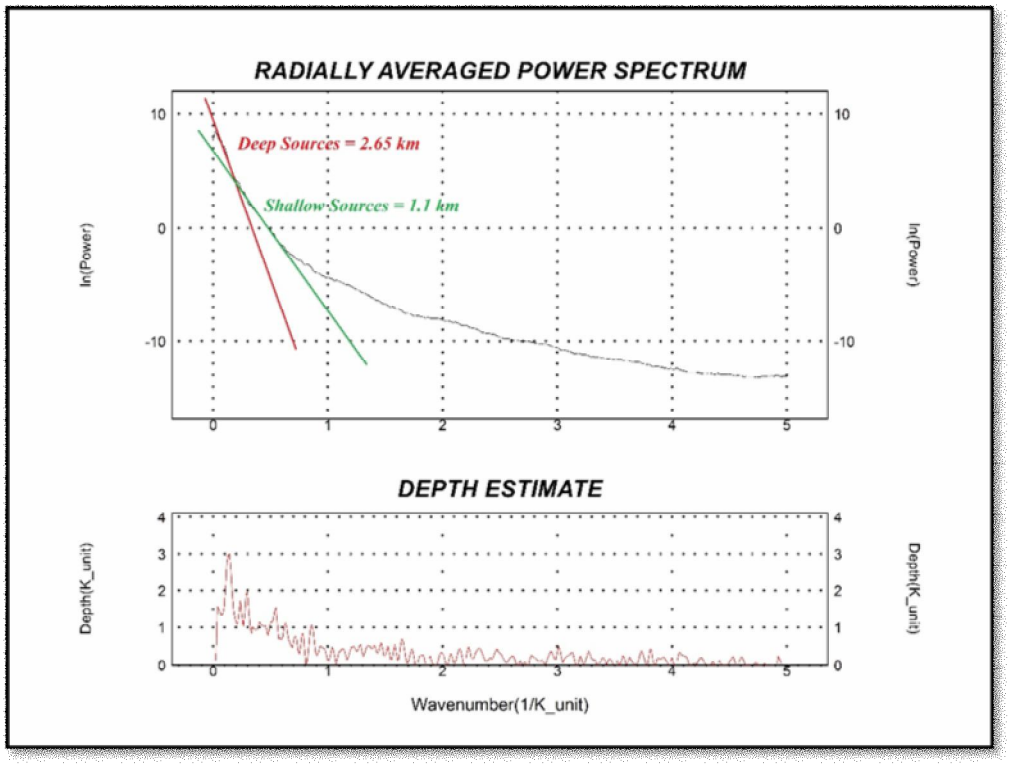

Fig. 8: Power spectrum curves of the aeromagnetic field-intensity data showing the corresponding average depths, Wadi Timsah area, Southern Eastern Desert, Egypt.

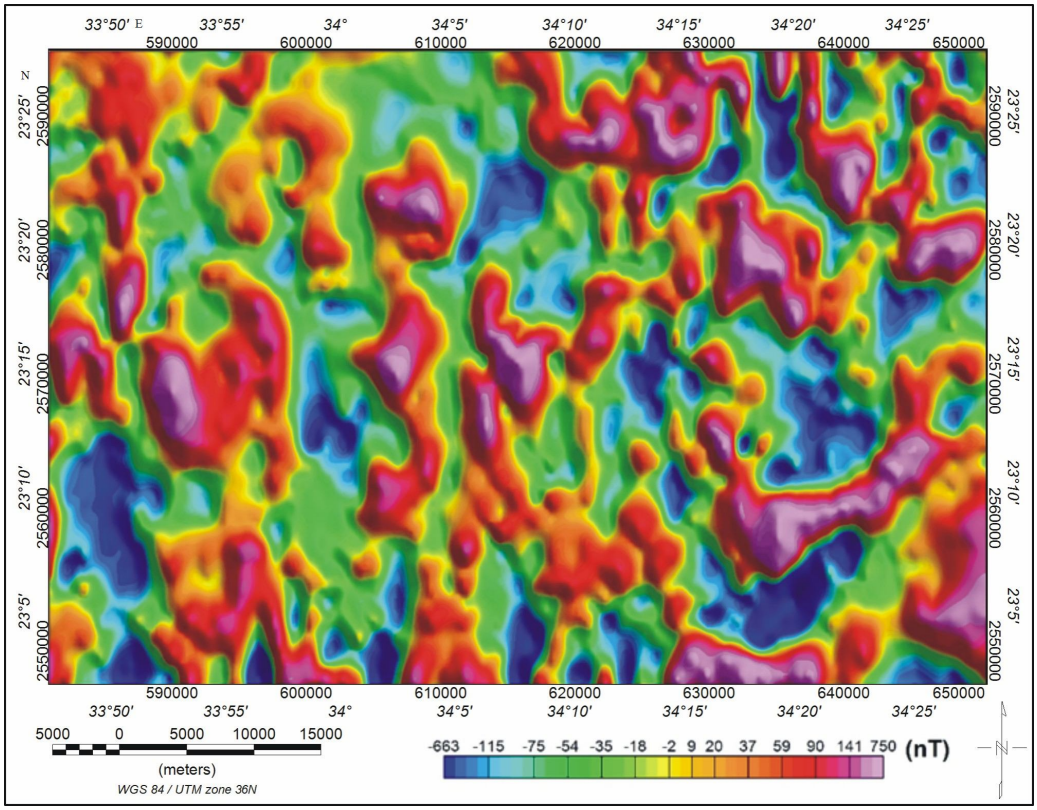

Fig. 9a: Shaded colour contours of the RTP residual aeromagnetic field-intensity map, Wadi Timsah area, Southern Eastern Desert, Egypt.

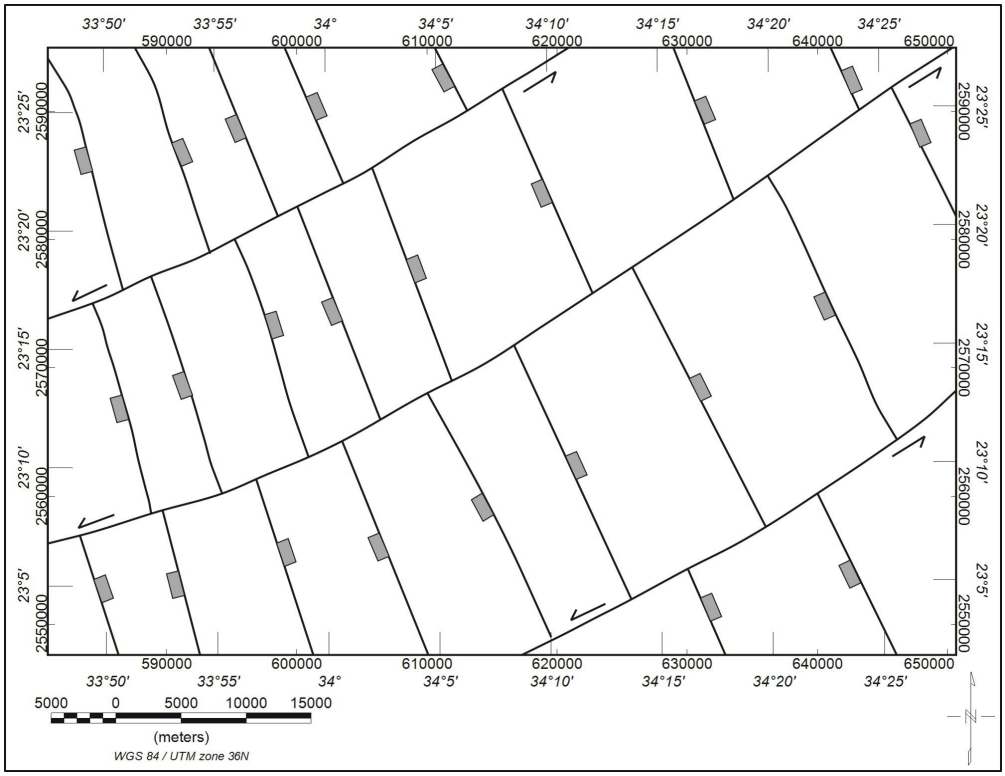

Fig. 9b: Shallow-seated structures, as concluded from the RTP residual aeromagnetic field-intensity map, Wadi Timsah area, Southern Eastern Desert, Egypt.

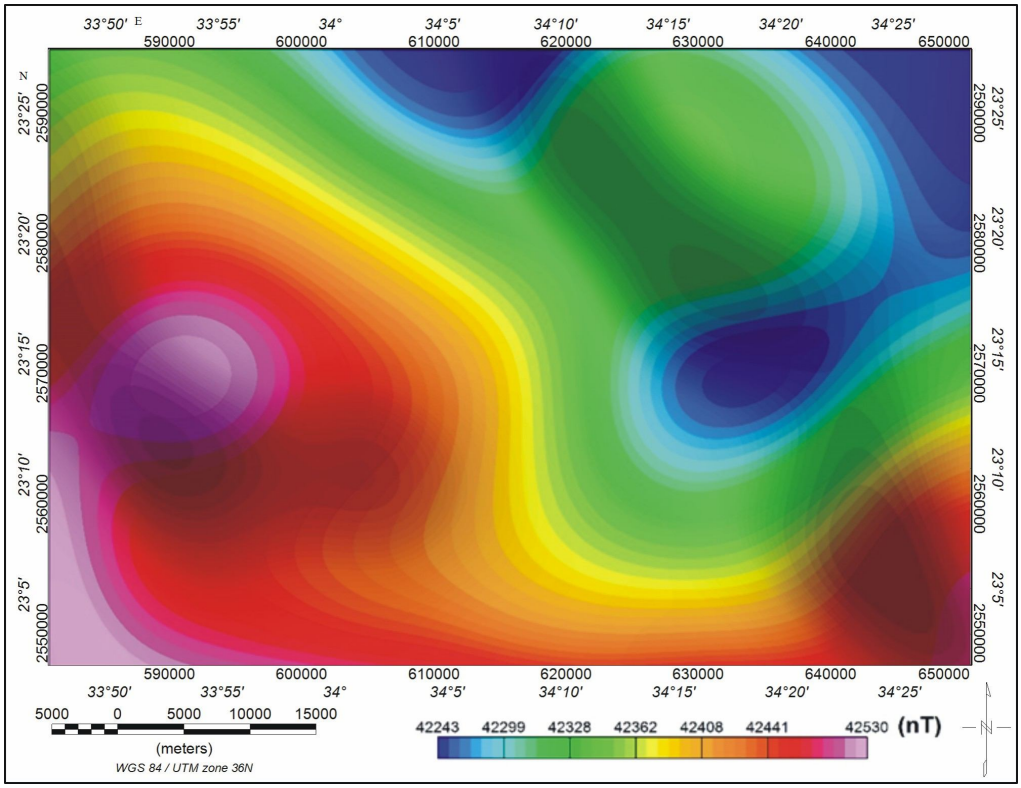

Fig. 10a: Shaded colour contours of the RTP regional aeromagnetic field-intensity map, Wadi Timsah area, Southern Eastern Desert, Egypt.

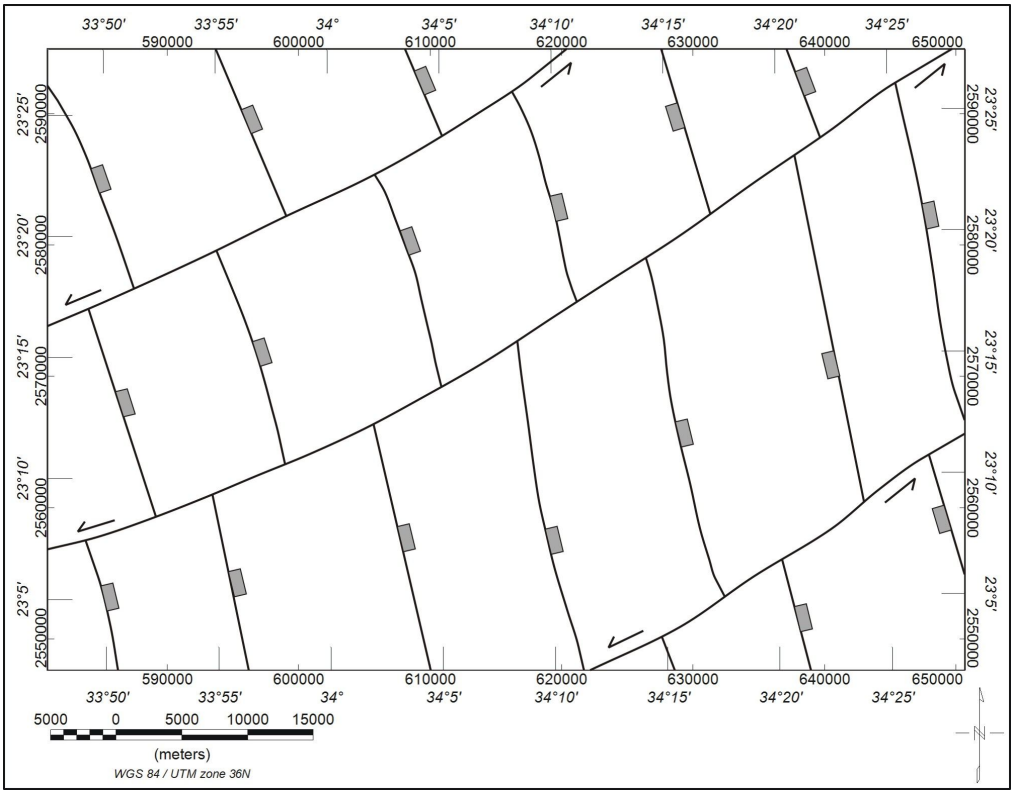

Fig. 10b: Deep-seated structures, as deduced from the RTP regional aeromagnetic field-intensity map, Wadi Timsah area, Southern Eastern Desert, Egypt.

The regional magnetic anomalies are strong, broad, extend over large areas and usually have high amplitudes and low frequencies. These anomalies are of considerable significance in the regional tectonic studies of the basement complex, and of secondary importance in mineral and petroleum explorations.

Most of the interpreted lineaments (faults and fractures) are trending in the NE-SW and NNW-SSE to NW-SE directions (Figs. 9b & 10b).

3.2.2 Analysis and interpretation:

Various methods were elaborated for estimating the source locations and other parameters from aerial magnetic field-intensity data, both in profile and grid forms. Two advanced techniques were used to analyse the magnetic data, as a guide for performing structural lineament interpretation. These methods include horizontal gradient magnitude (Cordell and Grauch, 1982& 1985 and Blakely and Simpson, 1986) and Euler deconvolution (Thompson, 1982; and Reid et al., 1990). They were proven as efficient tools to map the locations of magnetic structures, such as faults and contacts. Moreover, the Euler method provides depth estimates to these structures, beside their horizontal locations.

2.2.1. Horizontal gradient magnitude (HGM):

Horizontal gradient is a simple approach to locate linear structures, such as contacts and faults from potential field data. For a magnetic field, F, the horizontal gradient magnitude (HGM) is given by Cordell and Grouch, (1982 & 1985) as:

$$HGM = \sqrt{\left(\frac{\partial f}{\partial x}\right)^2 + \left(\frac{\partial f}{\partial y}\right)^2}$$

where, $\frac{\partial f}{\partial x}$ and $\frac{\partial f}{\partial y}$ represent the first- order derivatives of the magnetic field f in the x & y directions.

The peaks of this function occur over the magnetic contacts under certain assumptions:

(1) The magnetic field and source magnetization are vertical,

(2) The contact is vertical and

(3) The sources are thick (Phillips, 2000).

Violation of the first two assumptions leads to shift the peaks away from the contact location. Violation of the third assumption leads to secondary peaks parallel to that of the contact. When these assumptions are satisfied, the method is effective in detecting lineaments, that may correspond to basement faults and contacts. The significant advantage of the horizontal gradient method is its low sensitivity to the noise, in the data, because it only requires calculations of the two first-order horizontal derivatives of the field (Phillips, 1998). It is usually necessary to perform a

standard phase shift operation, known as Reduction-to-Pole (RTP) on the observed magnetic field, In order to partially satisfy the first two assumptions.

When applied to the RTP aeromagnetic data, the HGM (Cordell and Grauch, 1985; Blakely and Simpson, 1986; and Roest and Pilkington, 1993) assumes that, the sources are isolated and possess vertical contacts separating thick lithologic units. Peaks in the HGM method of the RTP aeromagnetic field are used to locate the vertical contacts and estimate their strike directions. Crests in the HGM grid can be traced by passing a small 3 by 3 window over the grid data and searching for maxima (Blakely and Simpson, 1986).

The HGM method provides contact locations, that are continuous, thin and straight (Fig. 11), compared to the RTP-TMI map (Fig. 12). The HGM map shows major anomalies in the N-S and ENE-WSW directions. These anomalies correspond to lithological contact zones, with large magnetic susceptibility differences. In order to highlight the contact directions, shown on the HGM map (Fig. 12), the maxima were delineated. This map reveals the structural complexity of the study area, such as faults cutting the basement rocks. For this reason, the HGM method was used to determine the locations of certain physical property (magnetization) boundaries.

2.2.2. Euler deconvolution method:

Depth estimation using the Euler deconvolution technique was applied to delineate lithologic contacts. This technique provides automatic estimates of the source locations and depths. This method is commonly employed in magnetic interpretation, because it requires only a little prior knowledge about the magnetic source geometry, and more importantly no information about the magnetization vector (Thompson, 1982; and Reid et al., 1990). Magnetic field (M) and its spatial derivatives satisfy the Euler's equation of homogeneity (Reid et al., 1990), shows as follow:

$$(x - x_0)\frac{\partial M}{\partial x} + (y - y_0)\frac{\partial M}{\partial y} + (z - z_0)\frac{\partial M}{\partial z} = N(B - M)$$

where

(B) is called the 'background' term, that describes the constant contribution of the regional field,

(x, y & z) are the coordinates of the observation points, at which the total magnetic field (M) is measured,

(x_0, y_0 & z_0) are the coordinates of the point sources of the causative bodies, as a function of M (x, y, z), and

the value (N) is referred to as the structural index (SI), that is an indicator of the geometry of a causative body.

The Euler deconvolution used the structural index as an exponential factor, that corresponds to the decay rate of the potential field, as a function of the distance between the source and the measurement point. This parameter is an indicator of the geometrical shape of the anomalous source. Selecting the correct structural index is crucial to achieving success, when applying this technique (Reid, 1995). Despite the fact that, the Euler deconvolution displays good locations for horizontal sources, an error in choosing the structural index can cause both inaccuracy in determining the depth of the source (Ravat, 1996; and Barbosa et al., 1999) and the dispersed solutions associated with the isolated anomalies (Silva et al., 2001).

In the present study, the structural index (SI≈0) of contact or step (Thompson, 1982 and Reid et al., 1990) was used, since the main objective of this study is to map faults and contacts. Despite of generating scattered solutions, using structural index very near to zero is the way for better estimation of depth and location of the contact/fault.

The Euler deconvolution method was applied to the RTP aeromagnetic field-intensity data. The 3D Euler solutions for the RTP-TMI map of the study area, at a structural index (SI≈0) were produced using Oasis montaj package (Geosoft program, 2007). After assigning the structural index (N), the system used the least squares method to solve the Euler's equation simultaneously for estimating the locations and depths of magnetic bodies.

The results of Euler solutions are presented on Fig. (13), which shows good clustering along the linear segments trending in the N-S, NNW-SSE, NE-SW and ENE-WSW directions. Moreover, these solutions provide depth estimates of these structures. The estimated depths varied between 215 m for the near-surface structures and 2800 m for the deep-seated structures.

These results of the two interpretation methods showed that, the Euler deconvolution confirms the results attained from the HGM under the assumption that, the edges of anomalous sources are caused by vertical contacts.

4. GEOLOGICAL AND INTERPRETED RADIOMETRIC AND MAGNETIC STRUCTURAL LINEAMENTS

The surface structural lineaments, were deduced from the geologic, radiometric and magnetic maps (Figs. 14a, 14b and 14c). This assisted in defining the principal structural trends that played the significant role in the study area. The general results obtained could be summarized in the following remarks.

The general trends that, as obtained from the geologic structures (Fig. 2), are illustrated on the rose diagram (Fig. 14a). This diagram shows that the WNW-ESE, NNE-SSW, ENE-WSW, NE-SW and NW-SE trends represent these structures on this map, arranged in a decreasing order of magnitude.

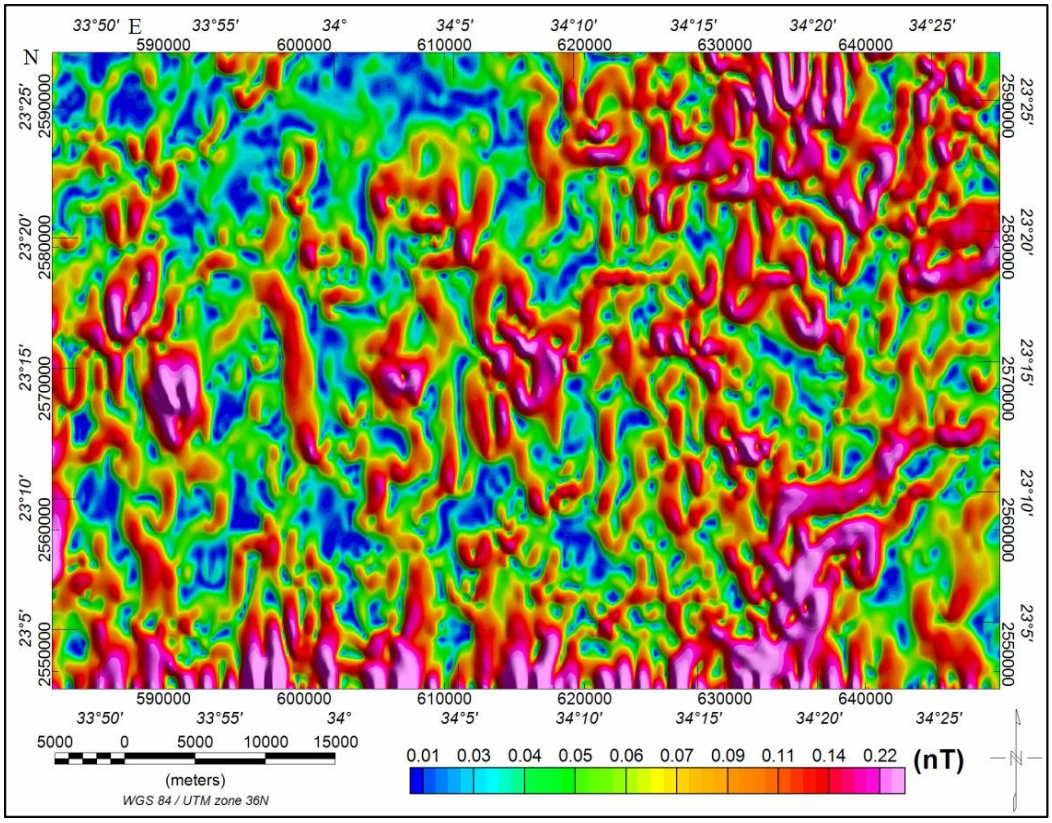

Fig. 11: Horizontal gradient magnitude (HGM) of the RTP aeromagnetic field-intensity map, Wadi Timsah area, Southern Eastern Desert, Egypt.

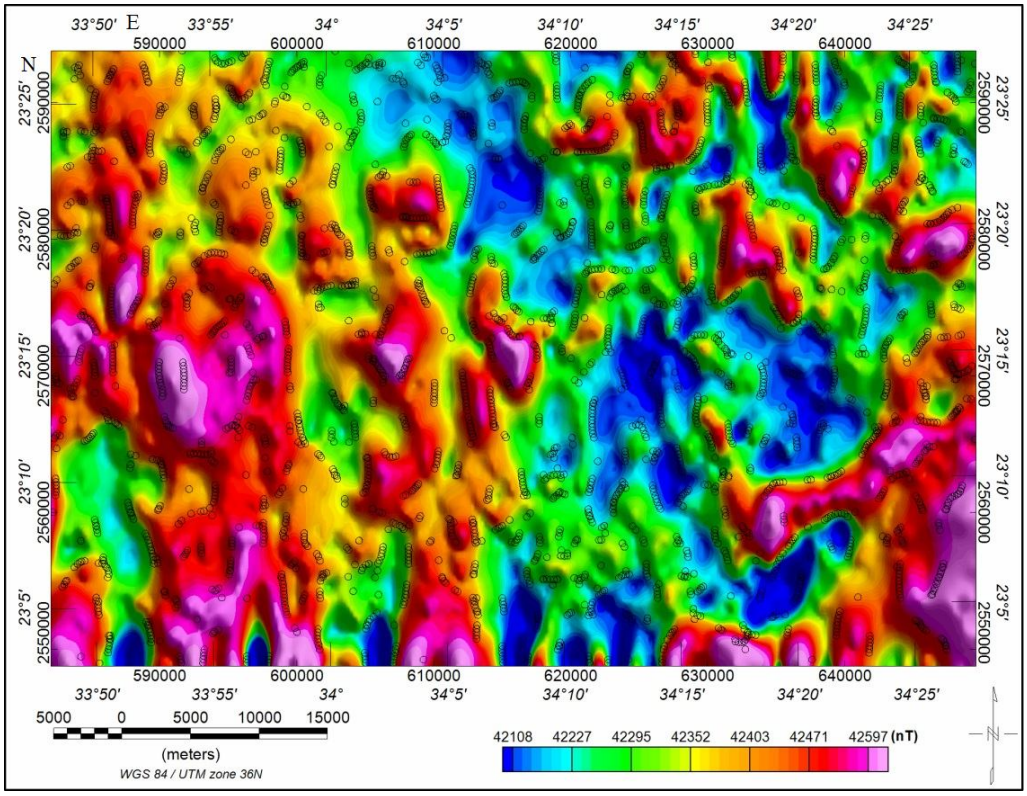

Fig. 12: Maxima of the horizontal gradient magnitudes, superimposed on the RTP aeromagnetic field-intensity map, Wadi Timsah area, Southern Eastern Desert, Egypt.

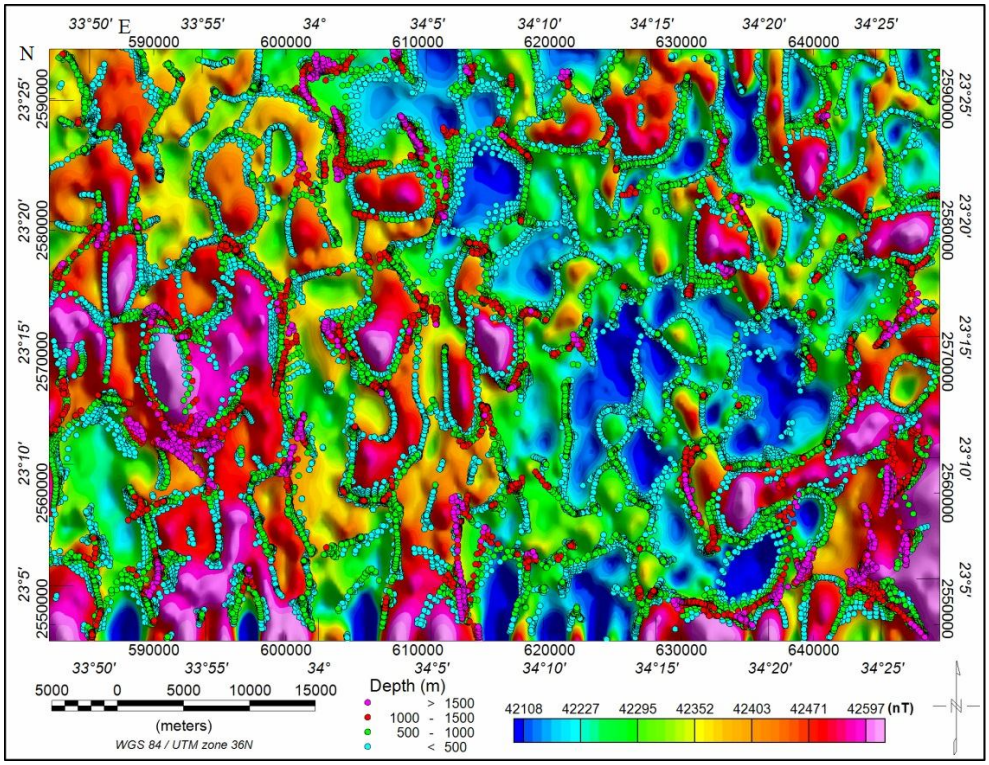

Fig. 13: Euler deconvolution solutions, superimposed on the RTP aeromagnetic field-intensity map, Wadi Timsah area, Southern Eastern Desert, Egypt.

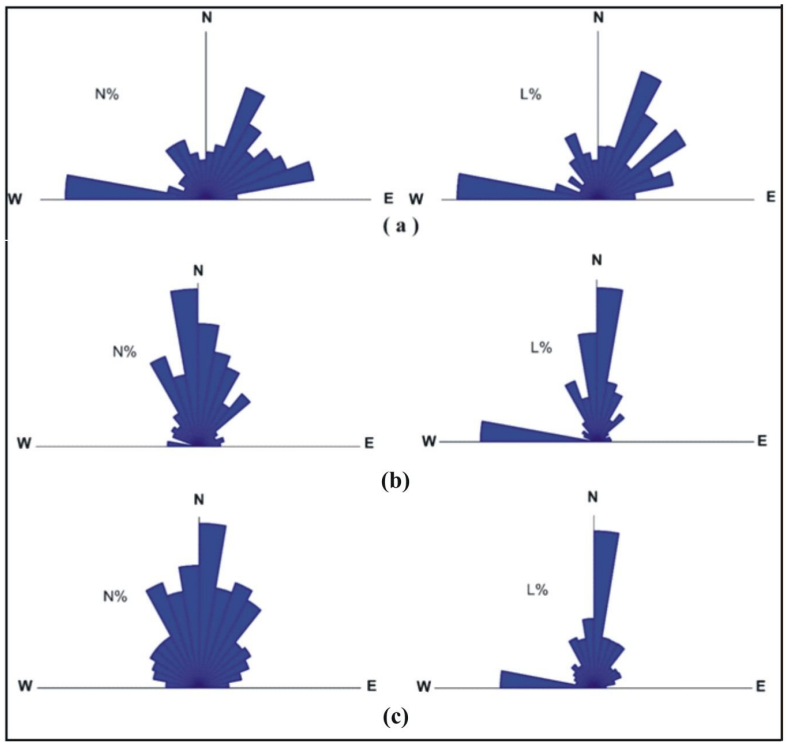

Fig. 14: Rose diagrams showing the main geological (original) and interpreted geophysical structural lineaments as deduced from (a) Geologic map (Fig. 2), (b) Maxima of the HGM map (Fig. 10), (c) Euler deconvolution map (Fig. 12), Wadi Timsah area, Southern Eastern Desert, Egypt. Frequency (N %) = the percent of total number of lines that fall within this trend and Length (L %) = percent of total lineaments lengths that are in that trend.

The structural lineaments as deduced from the T.C. aeroradiometric map (Fig. 3) are illustrated on Fig. (5). It shows that the NE-SW, NW-SE and NNW-SSE trends represent the main structures on this map.

The results of the aeromagnetic data were employed for the investigation of subsurface structure. The interpreted structural maps (Figs. 9b and 10b) played a considerable role in the representation of the near-surface and deep-seated faulting systems affecting the study area. They were deduced from the residual and regional magnetic data respectively (Figs. 9a and 10a). These maps show mainly two intersecting sets of NE-SW and NNW-SSE to NW-SE trending faults (Figs. 9b and 10b). The first interpreted group of faults comprises those with nearly NE-SW trends. These interpreted faults were interpreted as left-lateral strike-slip faults. The second interpreted group of faults includes those of nearly NNW-SSE and NW-SE direction. These faults represent the main trend of granite intrusion

The two rose diagrams of the Maxima of the horizontal gradient magnitude (HGM) map and Euler solutions map (Figs. 14b and 14c) show good similarity between their results. The structures affecting the investigated area have trends NNE-SSW, WNW-ESE, NE-SW and NW-SE.

Finally, two trends are encountered as strong trends (NE-SW and NNW-SSE) along the radiometric map (TC) and all magnetic maps. This means that these trends represent both shallow and deep-seated depths in the study area.

Moreover, through correlation of all structural lineament trends, as deduced from geologic, radiometric (TC) and magnetic (residual and regional) dataset; four significant trends were recorded as major ones (NE-SW, NNE-SSW, NW-SE and WNW-ESE). Therefore, these trends are considered the most significant trends in the study area from the radiometric and magnetic points of view.

5. CONCLUSIONS

The present study deals with the structural interpretation of the radiometric and magnetic survey data of Wadi Timsah area, Southern Eastern Desert, Egypt. These two methods were utilized in order to investigate the surface and subsurface features affecting the structural framework of the study area and to detect any relation that might exist between the radiometric anomalies and structures.

The results show that, the study area reflects high radioactivity level (more than 15 Ur), which is considered as the most important level from the radiometric point of view. It is recorded mostly over younger granites (monzogranites and alkali-feldspar granites) that located at the central and southeastern parts of the study area. The major linear trends associated with the radioactive anomalies follow the NE-SW, NW-SE, N-S and NNW-SSE directions.

Two techniques of analysis were applied on the aeromagnetic data with the aim to detect the locations and depths of the magnetic source edges as an aid to structural interpretation. These techniques include the Horizontal Gradient Magnitude (HGM) and the Euler Deconvolution. These two methods were applied to the RTP magnetic map. The HGM method could map the deep-seated and near-surface magnetic structures of the study area. The Euler solutions provide tracing of linear segments and the depths to these features. The estimated depths varied between 215m for the near-surface structures and 2800 m for the deep-seated ones.

The structural lineament trends, which were deduced from geologic, radiometric (TC) and magnetic datasets show four significant directions that, are recorded as major trends (NE-SW, NNE-SSW, NW-SE and WNW-ESE). Therefore, these trends are considered the most significant trends in the study area from the radiometric and magnetic points of view.

Acknowledgements:

The authors would like to express their gratitude to Dr. H. M. Youssef, Lecturer of geophysics, Exploration Division, Nuclear Materials Authority of Egypt, for his critical help and fruitful discussions during this work.

REFERENCES

Aero-Service, 1984: Final operational report of airborne magnetic / radiation survey in the Eastern Desert, Egypt. For the Egyptian General Petroleum Corporation (EGPC), Cairo, Egypt. Aero-Service Division, Western Geophysical Company of America, Houston, Texas, USA, Six Volumes.

Barbosa, V.C.E., Silva, J.B.C. and Medeiros, W.E., 1999: Stability analysis and improvement of structural index estimation in Euler deconvolution. Geophysics, V. 64 pp. 48–60.

Blakely, R.J. and Simpson, R.W., 1986: Approximating edges of source bodies from magnetic and gravity anomalies. Geophysics, V. 51, pp. 1494-1498.

Cordell, L. and Grauch, V.J.S., 1982. Mapping basement magnetization zones from aeromagnetic data in the San Juan Basin, New Mexico. 52nd Annual International Meeting, SEG Expanded Abstracts, pp. 246-247.

Cordell, L. and Grauch, V.J.S., 1985: Mapping basement magnetization zones from aeromagnetic data in the San Juan basin, New Mexico. In: Hinzc, W.J. (Ed.), The Utility of Regional Gravity and Magnetic Anomaly Maps: Soc. Expl. Geophys. , pp. 181-197.

Egsma, 1996: Geologic map of Gabal Had'b Quadrangle, Egypt, scale 1:250,000. Egyptian Geological Survey and Mining Authority (EGMA), Cairo, Egypt.

El-Gaby, S., List, F.K. and Tehrani, R., 1990: The basement complex of the Eastern Desert and Sinai. In: Said, R. (Ed.). The Geology of Egypt. Balkema, Rotterdam, Holland, pp. 175–184.

El-Shazly, E.M., 1977: The geology of the Egyptian region. In the Ocean Basins and Margins, Edited by Narin, A.E.M., Kanes, W.H., and Stehli, F.G., Plenum Publishing Corporation, pp. 379-444.

Geosoft Program (Oasis Montaj Package), 2007: Geosoft mapping and application system, Inc. Suit 500, Richmond St., West Toronto, ON Canada N5SIV6.

Hassan, M. A., and Hashad, A. H., 1990: Precambrian of Egypt. In The Geology of Egypt, R. Said (ed), A. A. Balkema, Rotterdam, Netherlands, pp. 201-245.

Kröner, A., (1984): Late Precambrian plate tectonics and orogeny: a need to redefine the term pan-African. In: Klerkx, J. and Michot, J. (Eds.): Geologie Africaine. African Geology, p. 23-28, Tervuren.

Phillips, J.D., 1998: Processing and interpretation of aeromagnetic data for the Santa Cruz Basin - Patahonia mountains area, South-Central Arizona. U.S. Geological Survey Open-File Report, Arizona, USA, pp. 2–98.

Phillips, J.D., 2000: Locating magnetic contacts: a comparison of the horizontal gradient, analytic signal, and local wavenumber methods. Soc. Explor. Geophys., Expanded Abstracts with Biographies, Technical Program, V. 1, pp. 402-405.

Ravat, D., 1996: Analysis of the Euler method and its applicability in environmental magnetic investigations. J. Environ. Eng. Geophys., V. 1, pp. 229–238.

Reid, A.B., 1995: Euler deconvolution: past, present and future – a review. In: 65th Annual International Meeting of the Society of Exploration Geophysicists, Houston, Texas, USA, pp. 272–273.

Reid, A.B., Alsop, J.M., Grander, H., Millet, A.J. azand Somerton, I.W., 1990: Magnetic interpretation in three dimensions using Euler deconvolution. Geophysics, V. 55, pp. 80-91.

Roest, W.R. and Pilkington, M., 1993: Identifying remnant magnetization effects in magnetic data, Geophysics, V.58, No.5, pp.653-659.

Silva, J.B.C., Barbosa, V.C.F. and Medeiros, W.E., 2001: Scattering, symmetry, and bias analysis of source position estimates in Euler deconvolution and its practical implications. Geophysics, V. 66, pp. 1149–1156.

Thompson, D.T., 1982: EULDPH-A technique for making computer-assisted depth estimates from magnetic data. Geophysics, V. 47, pp. 31-37.